Neuron
Article

Dopamine Neurons Control Striatal Cholinergic Neurons via Regionally Heterogeneous Dopamine and Glutamate Signaling

Nao Chuhma,[1,2,*] Susana Mingote,[1,2] Holly Moore,[1,3] and Stephen Rayport[1,2,*]
[1]Department of Psychiatry, Columbia University, New York, NY 10032, USA
[2]Department of Molecular Therapeutics
[3]Department of Integrative Neuroscience
NYS Psychiatric Institute, New York, NY 10032, USA
*Correspondence: nc2027@columbia.edu (N.C.), sgr1@columbia.edu (S.R.)
http://dx.doi.org/10.1016/j.neuron.2013.12.027

SUMMARY

Midbrain dopamine neurons fire in bursts conveying salient information. Bursts are associated with pauses in tonic firing of striatal cholinergic interneurons. Although the reciprocal balance of dopamine and acetylcholine in the striatum is well known, how dopamine neurons control cholinergic neurons has not been elucidated. Here, we show that dopamine neurons make direct fast dopaminergic and glutamatergic connections with cholinergic interneurons, with regional heterogeneity. Dopamine neurons drive a burst-pause firing sequence in cholinergic interneurons in the medial shell of the nucleus accumbens, mixed actions in the accumbens core, and a pause in the dorsal striatum. This heterogeneity is due mainly to regional variation in dopamine-neuron glutamate cotransmission. A single dose of amphetamine attenuates dopamine neuron connections to cholinergic interneurons with dose-dependent regional specificity. Overall, the present data indicate that dopamine neurons control striatal circuit function via discrete, plastic connections with cholinergic interneurons.

INTRODUCTION

In the striatum (Str), interactions between dopamine (DA) and acetylcholine (ACh) are central to the current understanding of movement and motivated behavior, major neuropsychiatric disorders, as well as to their pharmacotherapy (Benarroch, 2012). All Str DA arises from midbrain DA neurons, whereas all Str ACh arises from cholinergic interneurons (ChIs) (Goldberg and Wilson, 2010). DA and ACh appear to be in reciprocal balance (Do et al., 2012). ChIs comprise about 1% of striatal neurons, they are distributed throughout the striatum, their axons broadly influence striatal circuit function (Goldberg and Wilson, 2010; Kreitzer, 2009), and they are involved in associative learning, reward processing, and motor control (Schulz and Reynolds, 2013).

Midbrain DA neurons characteristically fire in bursts signaling unexpected reward and reward-related cues (Schultz, 2013). DA neuron bursts appear to pause ChI firing (Schulz and Reynolds, 2013) suggesting that DA neurons directly inhibit ChIs. Consistent with this, DA agonists inhibit ChI activity, via D2 receptors (Kreitzer, 2009). Although DA has been thought to function as a modulatory transmitter, the striking temporal relationships between DA neuron activity and ChI pauses argue that DA neurons convey discrete temporal information. DA neurons do make monosynaptic connections with ChIs (Dimova et al., 1993), yet functional connections of DA neurons to ChIs have not been described. Synchronized activation of ChIs can drive DA release via presynaptic nicotinic acetylcholine (nACh) receptors (Cachope et al., 2012; Threlfell et al., 2012); however, this is independent of DA neuron activity. Thus, the synaptic basis for the tightly orchestrated reciprocal relationship between DA neuron activity and ChI burst-pause sequences has not been clear.

DA neurons have differing functions across the Str domains they target (Belin et al., 2009; Di Chiara, 2002; Ikemoto, 2007; Kelly et al., 1975). They show target-dependent heterogeneity in their properties and firing patterns (Roeper, 2013). Heterogeneity extends to DA neuron transmission in the Str. DA neuron connections to spiny projection neurons (SPNs) in the nucleus accumbens (NAc) medial shell (m-shell) use glutamate as a cotransmitter, but not in the dorsal Str (dStr) (Hnasko et al., 2010; Stuber et al., 2010), whereas DA neuron connections to dStr SPNs use GABA as a cotransmitter (Tritsch et al., 2012). This heterogeneity likely extends to DA neuron connections to ChIs.

Here, we used optogenetics to examine the synaptic connections made by genetically identified presynaptic neuron populations—in this case DA neurons—with electrophysiologically identified Str target neurons. In mice with restricted expression of channelrhodopsin 2 (ChR2) in DA neurons, photostimulation of DA neuron synapses impinging on recorded ChIs revealed that DA neurons make direct and fast connections to ChIs with striking regional heterogeneity. This heterogeneity was accentuated following a single dose of amphetamine, pointing to the pivotal role of the connections in striatal circuit function.

RESULTS

Selective Activation of DA Neurons

To make DA neurons and their axon terminals activatable selectively, we injected a cre-inducible adeno-associated virus (AAV),

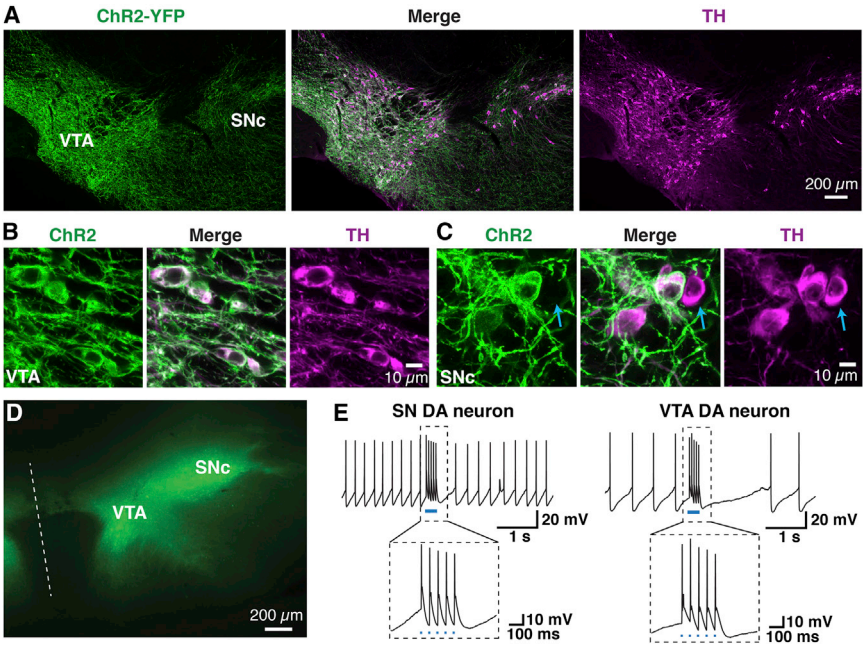

Figure 1. Selective Expression of ChR2 in Ventral Midbrain DA Neurons

(A–C) Double immunostaining for ChR2-EYFP (green, left) and TH (magenta, right) of SNc and VTA in AAV-DIO-ChR2-YFP injected DAT-IRES-cre mice (merged images are shown in the middle). (A) The VTA and medial SN are shown at low magnification. (B and C) Representative regions in the SNc (B) and in the VTA (C) are shown at high magnification. Arrows in (C) indicate a TH-positive ChR2-negative neuron.

(D) Direct YFP fluorescence is shown in a horizontal slice used for electrophysiological recording. The dashed line indicates the midline.

(E) Confirmation of DA neuron responses to train photostimulation, five pulses at 20 Hz, in the SN (left) and in the VTA (right). Photostimulation (blue bars) reliably generated action potentials (photostimulation time interval is outlined in dashes and expanded below).

See also Figure S1.

with double-floxed inverted open reading frame (DIO) containing *ChR2* fused to enhanced yellow fluorescent protein (*EYFP*) (Atasoy et al., 2008; Tsai et al., 2009), into the ventral midbrain of DAT-IRES-cre mice (Bäckman et al., 2006). To confirm specific expression in DA neurons, we immunostained for the DA neuron marker tyrosine hydroxylase (TH) and for ChR2-EYFP (Figures 1A–1C). Because TH has a cytoplasmic distribution (Figures 1A–1C, right, magenta) and ChR2-EYFP a membrane distribution (Yizhar et al., 2011) (Figures 1A–1C, left, green), DA neurons expressing ChR2-EYFP were identified as magenta cells outlined in green (Figures 1A–1C, middle). Most TH-positive neurons showed EYFP expression, both in the ventral tegmental area (VTA) (Figure 1B) and substantia nigra pars compacta (SNc) (Figure 1C). To confirm specificity of ChR2 expression in DA neurons, we counted ChR2-positive cells and found that 99.9% of ChR2-EYFP-positive neurons were TH positive (n = 1,308); only one ChR2-EYFP-positive cell was TH negative. We counted GABA neurons (n = 42), identified by immunostaining for glutamate decarboxylase (GAD) 67, and ChR2-YFP-positive neurons (n = 100); no GAD-positive cells were ChR2-EYFP positive (Figure S1 available online). Thus, ChR2 expression was specific to DA neurons, and not seen in VTA GABA neurons known to project to ChIs (Brown et al., 2012). In acute ventral midbrain slices, ChR2-EYFP expression was visualized by direct fluorescence (Figure 1D). Train photostimulation of five pulses at 20 Hz (5 ms pulse duration) reliably drove DA neurons to fire in both the VTA and SNc (Figure 1E).

DA Neuron Synaptic Input to ChIs in Three Striatal Domains

We recorded from ChIs in three functional Str domains, the dStr, NAc core, and m-shell (Figure 2A). ChIs were identified as large, tonically firing cells with a hyperpolarization-activated cation channel current (I_h) (Goldberg and Wilson, 2010) (Figure S2A). Immunostaining revealed that all cells with these characteristics were choline acetyltransferase (ChAT) positive (n = 17), confirming the electrophysiological identification (Figure S2B). Single-pulse photostimulation of DA neuron terminals at 0.1 Hz elicited a hyperpolarization in ChIs in the dStr (−2.22 ± 0.93 mV, n = 9 cells), little response in ChIs in the core (0.89 ± 0.63 mV, n = 10 cells), and a strong depolarization with action potential generation in ChIs the m-shell (4.43 ± 0.86 mV, n = 10 cells) (Figure 2B). Responses in ChIs in the dStr and the m-shell were significantly different (p = 0.044, p = 0.001, respectively, one-sample t test, compared to baseline), but not in the core (p = 0.19). ChIs showed no significant regional differences in either resting membrane potential (dStr, −64.0 ± 1.4 mV; core, −61.5 ± 1.7 mV; m-shell, −61.1 ± 1.5 mV; p = 0.38, one-way ANOVA) or action potential threshold (dStr, −51.9 ± 1.6 mV; core, −50.6 ± 1.8 mV; m-shell, −47.0 ± 1.5 mV; p = 0.08). Baseline firing frequencies of ChIs were 2.5 ± 0.4 Hz (n = 16 cells) in the dStr, 5.9 ± 1.0 Hz (n = 12 cells) in the core and 3.8 ± 0.6 Hz (n = 17 cells) in the m-shell, and significantly higher in the core than the other two subregions (p = 0.004, one-way ANOVA with Scheffe's post hoc test), suggesting some regional heterogeneity in ChI excitability.

We measured the latency of responses of ChIs to DA neuron terminal photostimulation. The latency of the excitatory postsynaptic potential (EPSP) in the m-shell was 4.0 ± 0.4 ms, whereas that of the IPSP in the dStr was 8.0 ± 1.4 ms, which was significantly longer (p = 0.021, unpaired t test) (Figure 2C). The latency of PSPs was tightly distributed in each neuron, in both the dStr (Figure 2D, top traces, green circles) and the m-shell (Figure 2D, bottom traces, magenta circles). Cell 5 showed a wider distribution of latencies, with a shorter latency due to cell firing (Figure 2D, bottom traces). The EPSP in m-shell ChIs had the same latency as seen for EPSPs in SPNs (Stuber et al., 2010; Tecuapetla et al., 2010). Recordings from DA neuron axons connecting to SPNs revealed a delay of about 5 ms between photostimulation and generation of a presynaptic action current

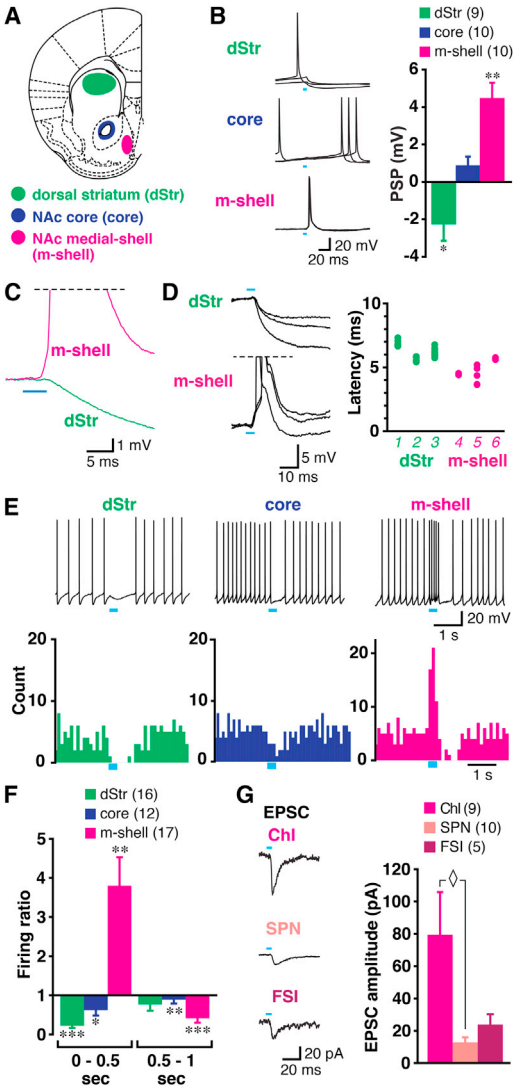

Figure 2. Photostimulation of DA Neuron Terminals Drives Regionally Heterogeneous Synaptic Responses in ChIs

(A) Recordings were made in the dStr (green), the NAc core (dark blue) and the NAc m-shell (magenta).

(B) PSPs evoked by single-pulse photostimulation (0.1 Hz, 5 ms duration; blue bars) in ChIs were recorded in the three regions (three traces are shown superimposed); the summary of PSP amplitudes is shown on the right. Negative values indicate hyperpolarization; numbers of recorded cells are in parentheses. PSP amplitudes differing significantly from baseline (0 mV) are indicated, respectively, by *p < 0.05 and **p < 0.01, by one-sample t test.

(C) Expanded view of the onset of PSPs recorded in the dStr and the m-shell. Averages of ten traces are shown. Action potentials are truncated (horizontal dashed line).

(D) Onset of three individual PSPs is shown superimposed, with the latency from the onset of photostimulation summarized for three cells in each region. Cell identification number (1–6) is in italics. Each closed circle is the measurement from a single trace; eight to ten traces were measured per cell (many circles overlap).

(E) Effect on ChI firing of photostimulation mimicking DA neuron bursting (five pulses at 20 Hz) in the three regions. Sample traces from each region are shown (top), with peristimulus histograms made from ten consecutive traces (0.1 s bin) (below). Blue bars indicate timing of train photostimulation.

(Tecuapetla et al., 2010), indicating that the latency for excitatory postsynaptic currents (EPSCs) in ChIs mainly reflects the activation time of ChR2 (Prakash et al., 2012). Factoring this in with the tight distribution of latencies, the m-shell ChI response is monosynaptic. The latency of the IPSP in dStr ChIs was about 4 ms longer, but also a showed a tight distribution, and is thus also likely to be monosynaptic.

We then used train photostimulation of DA neuron synapses (five pulses at 20 Hz) to mimic the DA neuron burst firing associated with reward-related cues (Schultz, 2013). In the dStr, this train photostimulation produced a hyperpolarization and a pause in firing in all recorded ChIs (Figure 2E, left). In the core, train photostimulation slowed firing, but did not produce an obvious pause (Figure 2E, middle). In the m-shell, train photostimulation drove ChIs to fire in bursts (Figure 2E, right), and then to fire more slowly or to pause. Train photostimulation of DA neuron synapses reliably drove a burst in all recorded m-shell ChIs. To evaluate the DA neuron-evoked synaptic response independent of variability in baseline ChI firing, we determined a firing ratio comparing firing frequency during train photostimulation (0–0.5 s from the onset of train) to the preceding 2 s of baseline firing. In the dStr, the firing ratio during train photostimulation was 0.22 ± 0.06 (n = 16, Figure 2F), which was significantly attenuated ($p < 0.001$, compared to baseline [ratio of 1], one-sample t test). In the core, the firing ratio during train photostimulation was 0.62 ± 0.13 (n = 12), also significantly reduced ($p = 0.015$; Figure 2F). In contrast, train photostimulation in the m-shell elicited burst firing in ChIs; the firing ratio during train photostimulation was 3.80 ± 0.72 (n = 17), which was significantly increased ($p = 0.001$; Figure 2F). In the dStr, in the subsequent half-second window (0.5–1 s from the onset of the train), the firing ratio was not significantly different from baseline (firing ratio 0.76 ± 0.16, $p = 0.16$), as a result of the variable duration of the pause and rebound firing (Figure S2C). In the core, the significant reduction in firing persisted (0.58 ± 0.10, $p = 0.002$). Firing was reduced (0.41 ± 0.12, $p < 0.001$) in the m-shell, as a result of a postburst hyperpolarization (PBH) (Figure S2C).

We next focused on excitatory DA neuron inputs to ChIs in the m-shell, comparing responses in the principal neuron types. We recognized ChIs, SPNs, and fast-spiking GABAergic interneurons (FSIs) by soma size, confirmed by their distinctive firing patterns (Figure S2A). Single-pulse photostimulation in the m-shell under voltage clamp (at −70 mV) elicited EPSCs (Figure 2G) that measured 79.5 ± 26.3 pA in ChIs, 12.8 ± 3.1 pA in SPNs, and 24.2 ± 6.3 pA in FSIs. This confirmed the previously reported smaller amplitude of EPSCs in SPNs (Stuber et al., 2010; Tecuapetla et al., 2010); responses in ChIs were significantly larger (Figure 2G, right, $p = 0.022$, one-way ANOVA with Scheffe's

(F) Ratio of firing during train (0–0.5 s from onset of train, left) and just after train photostimulation (0.5–1 s from onset, right) to baseline firing (firing ratio). Significant changes from baseline firing (ratio 1) are indicated by *p < 0.05, **p < 0.01, and ***p < 0.001 by one-sample t test, respectively.

(G) Comparison of fast EPSCs generated by single-pulse photostimulation among three cell types in the m-shell. Sample traces recorded from a ChI, SPN, and FSI are shown (left); traces are averages of ten consecutive traces. In a summary of EPSC amplitudes (right), ◇ indicates p < 0.05 by one-way ANOVA with Scheffe's post hoc test.

Data are presented as mean ± SEM. See also Figure S2.

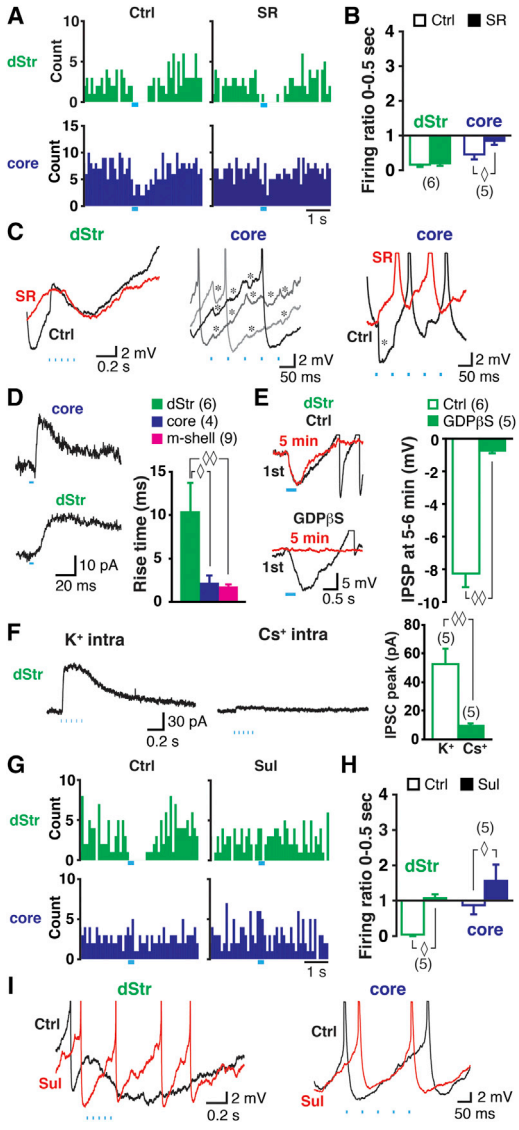

Figure 3. Neurotransmitter Mediation of the Pause in the dStr and Firing Attenuation in the Core

(A–C) Effect of the $GABA_A$ antagonist SR95531 (10 μM). Peristimulus histograms of firing under control (Ctrl) and after application of SR95531 (SR), in the dStr and the core are shown (A). Blue bars indicate train photostimulation. In a summary of firing ratios (B), ◇ indicates $p < 0.05$ by Wilcoxon signed ranks test. Numbers of recorded cells are in parentheses. Expanded sample traces (C) of responses to train photostimulation are shown for control (black) and after application of SR95531 (red), in the dStr and in the core. Middle panel shows three superimposed control traces with probable GABAergic IPSPs (*). Action potentials were truncated.

(D–F) The hyperpolarization in the dStr was G protein coupled and K^+ channel mediated. Sample traces of IPSCs evoked with a single light pulse are shown for the core and dStr (D, left). IPSCs are the average of ten traces. In measurements of the rise time (from 10% to 90% peak amplitude; D, right), ◇ and ◇ ◇ indicate $p < 0.05$ and $p < 0.01$, respectively, by one-way ANOVA with Scheffe's post hoc test. Intracellular 1–1.5 mM GDPβS blocked the IPSP in the dStr (E). The first trace (black) and the trace 5 min after entering whole-cell mode (red) are shown with control intracellular solution and with GDPβS (E, left). In a comparison of average IPSP amplitude at 5–6 min in control and with GDPβS (E, right), ◇ ◇ indicates $p < 0.01$ by Mann-Whitney U test. With Cs^+-based intracellular solution, IPSCs (holding at −60 mV) were blocked (F). IPSC traces at 5 min after entering whole-cell mode evoked by a train photostimulation with K^+ (F, left) and Cs^+ (F, middle) intracellular solution are shown. In a comparison of IPSC peak amplitude at 5–6 min after entering whole-cell mode (F, right), ◇ ◇ indicates $p < 0.01$ by Mann-Whitney U test.

(G and H) Effect of D2 antagonist sulpiride (10 μM). Peristimulus histograms of firing under control and after application of sulpiride, in the dStr and the core are shown (G). In a summary of firing ratios (H), ◇ indicates $p < 0.05$ by Wilcoxon signed ranks test. Expanded sample traces for control (black) and after sulpiride (red) are shown.

Data are presented as mean ± SEM. See also Figure S3.

post hoc test, between ChI and SPN). Compared to SPNs (−93.5 ± 2.7 mV) or FSIs (−79.9 ± 6.7 mV), ChIs have more depolarized resting membrane potentials (−61.1 ± 1.5 mV). Together with the larger EPSCs, DA neuron input to m-shell ChIs can drive them to fire, independent of coincident excitatory input. Thus, fast excitatory DA neuron transmission in the m-shell most potently affects ChIs.

Pharmacology of Inhibitory DA-Neuron Synaptic Responses in ChIs

Next, we examined the neurotransmitter mediation of inhibitory DA neuron connections to ChIs. In the dStr and in the core, train stimulation of DA neuron terminals reduced ChI firing. DA neuron GABA cotransmission observed in SPNs in the dStr (Tritsch et al., 2012) might contribute to the firing reduction. However, the $GABA_A$ antagonist SR95531 (gabazine; 10 μM) had no effect on the DA neuron-mediated inhibition of ChI firing in the dStr (control 0.16 ± 0.06, SR 0.21 ± 0.08, n = 6 cells, p = 0.46, Wilcoxon signed ranks test), whereas SR95531 attenuated the DA neuron-mediated inhibition of ChI firing in the core (firing ratio control 0.45 ± 0.14, SR 0.86 ± 0.13, n = 5 cells, p = 0.043) (Figures 3A and 3B). Baseline firing frequency was not affected by SR95531 in either the dStr (control 2.2 ± 0.4 Hz, SR 2.8 ± 0.6 Hz, p = 0.35) or the core (control 4.4 ± 0.3 Hz, SR 4.4 ± 1.3 Hz, p = 0.89). Thus, the effect of SR95531 in the core was not due to an increase in baseline firing as a result of blocking tonic GABA.

In the dStr, SR95531 application did not affect the DA neuron-driven ChI hyperpolarization (Figure 3C, left). In the core, some ChIs showed fast and small hyperpolarizations (Figure 3C, middle); these were blocked by SR95531 (Figure 3C, right), consistent with GABA cotransmission (Tritsch et al., 2012), mediated by $GABA_A$ receptors. The lack of a $GABA_A$ antagonist effect in the dStr also excludes a polysynaptic GABAergic contribution. Considering the relatively short latency of the hyperpolarization in the dStr (Figures 2C and 2D), only DA neuron glutamate cotransmission could drive local GABA neurons. The lack of an AMPA/kainate antagonist effect (CNQX, 40 μM) on the pause (firing ratio control 0.20 ± 0.12, CNQX 0.19 ± 0.09, n = 6, p = 0.465, Figure S3A) argues further against a polysynaptic GABAergic contribution.

To elucidate the mechanism of the longer latency response in the dStr, we measured activation time, as the 10%–90% rise time of synaptic responses, under voltage clamp (holding potential = −70 mV) with single-pulse photostimulation at 0.1 Hz (Figure 3D) and compared it to ChIs in the core that showed fast IPSCs (Figure 3D, left top). In the dStr, all ChIs showed slow

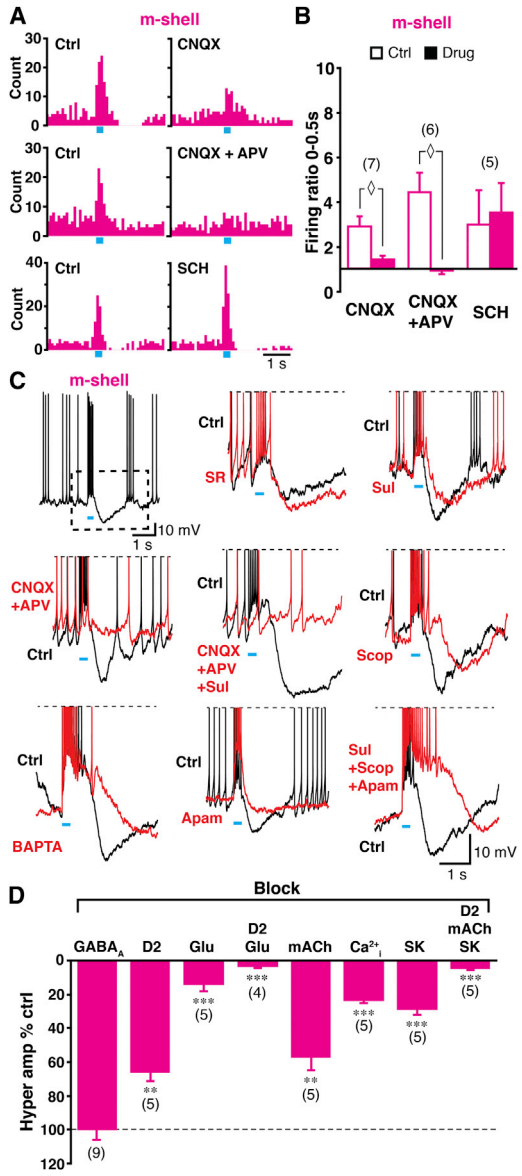

Figure 4. Neurotransmitter Mediation of Burst and PBH in the m-shell

(A and B) Pharmacology of burst. Effects of AMPA/kainate antagonist CNQX (40 μM), a cocktail of CNQX + NMDA antagonist D-APV (100 μM) and D1 antagonist SCH23390 (10 μM) are shown in peristimulus histograms (A) and firing ratios (B). ◇ indicates $p < 0.05$ by Wilcoxon signed ranks test.

(C and D) Pharmacology of PBH. The first sample trace shows the burst followed by PBH (C, top left). The PBH (dashed rectangle outline) is expanded in the subsequent panels. Sample traces show control PBH (black) and after drug application (red). Drugs tested were (from top middle to bottom right) SR95531, sulpiride, a cocktail of CNQX + D-APV, CNQX+D-APV+sulpiride, scopolamine, intracellular BAPTA, apamin, and a cocktail of sulpiride+ scopolamine+apamin. The percentage reduction in the PBH amplitude for each of the drugs is shown (D). The dashed line indicates control (no change). $^{**}p < 0.01$ and $^{***}p < 0.001$, respectively, with one-sample t test.

Data are presented as mean ± SEM.

IPSCs (Figure 3D, left bottom). The rise time was 10.5 ± 3.3 ms (n = 6 cells) in the dStr compared to 2.2 ± 0.8 ms (n = 4 cells) in the core. In further comparison, the rise time for EPSCs in the m-shell was 1.8 ± 0.2 ms (n = 9 cells). The rise time in the dStr was significantly longer than in the core (p = 0.042, one-way ANOVA with Scheffe's post hoc test), or m-shell (p = 0.009; Figure 3D, right), arguing against ionotropic transmitter receptor mediation of the dStr response.

When postsynaptic G proteins were inactivated selectively in dStr ChIs with intracellular GDPβS (1–1.5 mM), the hyperpolarization evoked by train photostimulation in the dStr was blocked 5 min after entering whole-cell mode (average amplitude at 5–6 min 0.73 ± 0.17 mV, n = 5 cells, Figure 3E), in contrast to recordings with control pipette solution (average amplitude at 5–6 min was 8.2 ± 0.8 mV, n = 6 cells; p = 0.004, Mann-Whitney U test). Train photostimulation evoked large IPSCs at a holding potential of −60 mV with K^+-based pipette solution (52.4 ± 10.9 pA, n = 5; Figure 3F). They were greatly reduced with a Cs^+-based pipette solution (9.3 ± 1.8 pA, n = 5, p = 0.008), consistent with mediation by G protein-activated inward rectifier K^+ channels (GIRKs), and not by $GABA_A$ receptors, which flux Cl^- and are not blocked by intracellular Cs^+. Thus, the hyperpolarization in the dStr was mediated through G protein coupling to K^+ channels.

The pause in the dStr could be mediated by D2 or $GABA_B$ receptors. We found that the D2 antagonist sulpiride (10 μM) blocked the pause (firing ratio control 0.04 ± 0.04, sulpiride 1.1 ± 0.1, n = 5 cells, p = 0.043) (Figures 3G and 3H) by blocking the hyperpolarization (Figure 3I, left), whereas the $GABA_B$ antagonist CGP55845 (3 μM) had no effect (firing ratio control 0.05 ± 0.04, CGP 0.06 ± 0.04, n = 5 cells, p = 0.99, Wilcoxon signed-ranks test; Figure S3B). In the core, sulpiride changed the attenuation of firing to a slight increase in firing (control 0.93 ± 0.3, sulpiride 1.4 ± 0.3, n = 5 cells, p = 0.043) (Figures 3G–3I, right). Baseline firing frequency was not affected by sulpiride, either in the dStr (control 2.1 ± 0.6 Hz, sulpiride 1.9 ± 0.6 Hz, p = 0.35), or in the core (control 5.6 ± 1.6 Hz, sulpiride 4.4 ± 1.4 Hz, p = 0.08). Thus, in the dStr, the pause was mediated by D2 receptors, whereas in the core the attenuation in firing was mediated by both D2 and $GABA_A$ receptors.

Pharmacology of Excitatory DA Neuron-Synaptic Responses in ChIs

In the m-shell, train photostimulation of DA neuron terminals drove ChI burst firing. DA neurons drive fast glutamatergic EPSCs in m-shell SPNs (Chuhma et al., 2004; Hnasko et al., 2010; Stuber et al., 2010; Tecuapetla et al., 2010) and could similarly drive ChIs. CNQX reduced the burst significantly (firing ratio control 2.8 ± 0.4, CNQX 1.4 ± 0.2, n = 7 cells; p = 0.018; Figures 4A and 4B), although a slight increase in firing remained after CNQX application. This remaining excitation was blocked by the NMDA antagonist D-APV (100 μM); firing ratio control 4.4 ± 0.9; CNQX+APV 0.92 ± 0.16, n = 6 cells, p = 0.028; Figures 4A and 4B). ChIs express DA D5 receptors (Rivera et al., 2002) that mediate excitation (Yan and Surmeier, 1997); however, the D1/D5 antagonist SCH23390 (10 μM) did not reduce the burst in m-shell ChIs (firing ratio control 3.0 ± 1.5, SCH 3.6 ± 1.4, n = 5 cells, p = 0.23; Figures 4A and 4B). Baseline firing was

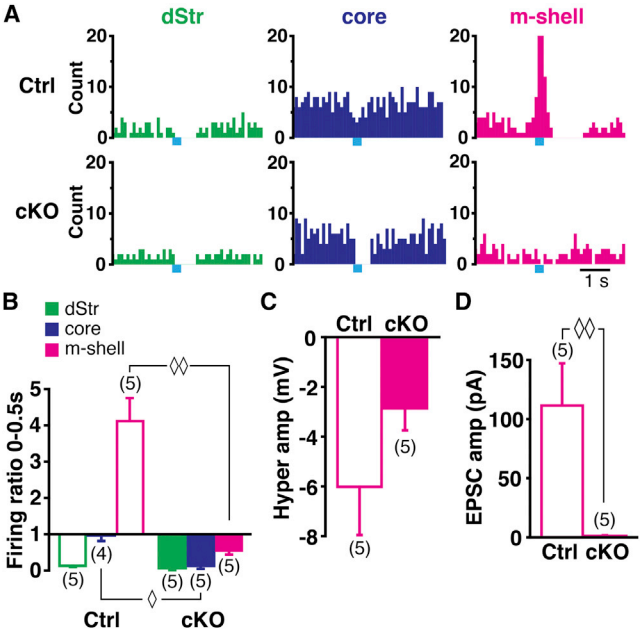

Figure 5. cKO of VGLUT2 in DA Neurons Eliminates Burst Firing and Reduces Regional Heterogeneity

(A) Peristimulus histograms of firing in the three regions in control (top) and in VGLUT2 cKO (bottom) slices.

(B) Firing ratio comparison between control and cKO in three regions.

(C) PBH amplitude appears diminished in cKO, but this was not significant.

(D) EPSCs evoked by single-pulse photostimulation are absent in cKO, showing the complete block of DA neuron glutamate cotransmission in cKO. ◇ and ◇◇ indicate $p < 0.05$ and $p < 0.01$, respectively, by Mann-Whitney U test.

Data are presented as mean ± SEM.

not affected by any of the applied antagonists (control 3.2 ± 0.7 Hz, CNQX 4.6 ± 1.3 Hz, p = 0.08; control 2.4 ± 0.3 Hz, CNQX+APV 2.1 ± 0.2 Hz, p = 0.67; control 5.0 ± 2.7 Hz; SCH 3.5 ± 1.3 Hz, p = 0.14). Thus, the burst in the m-shell was glutamate-mediated with little D5 contribution.

Following photostimulation of DA neuron terminals, most m-shell ChIs showed a PBH (Figures S2C, 4C, and 4D), which could be mediated by GABA cotransmission or activation of GABA interneurons via glutamate cotransmission. However, the $GABA_A$ antagonist SR95531 did not affect the PBH (100.3% ± 5.8% of control, n = 9 cells, p = 0.96, one-sample t test; Figures 4C and 4D). In contrast to the D2 mediation of the pause in the dStr, sulpiride did not block the PBH in m-shell ChIs, although it reduced the amplitude significantly (66.0% ± 5.3% of control, n = 5 cells, p = 0.003; Figures 4C and 4D). The PBH was reduced to 13.9% ± 3.8% of control by glutamate blockade with CNQX and D-APV together (n = 5 cells, p = 0.003), and blockade of both glutamate and D2 receptors almost completely eliminated the PBH (3.1% ± 1.4% of control, n = 4 cells, p < 0.001; Figures 4C and 4D). The PBH was reduced more significantly with a cocktail of D2 and glutamate blockers than with glutamate blockers alone (p = 0.032, Mann-Whitney U test), arguing that the PBH was mediated mainly by activity-dependent components, but partially by D2 receptors.

Activity dependence could involve muscarinic acetylcholine (mACh) autoreceptors (Kreitzer, 2009). However, a high concentration of mACh antagonist scopolamine (10 μM) had only a small, although significant effect on the PBH (57.1% ± 7.7% of control, n = 5, p = 0.009, one-sample t test; Figures 4C and 4D). More likely, the activity dependence of the PBH was mediated by small conductance Ca^{2+}-dependent K^+ channels (SK channels) (Goldberg and Wilson, 2010); to test this, we blocked activation of SK channels by chelating intracellular Ca^{2+} with BAPTA (10 mM) in the patch pipette. About 15 min was required for BAPTA to show a full effect, so the first 5 min after entering whole-cell mode served as a control. BAPTA strongly attenuated the PBH (23.1% ± 1.8% of control, n = 5, p < 0.001; Figures 4C and 4D). Bath application of the SK channel antagonist apamin (300 nM) strongly attenuated the PBH (29.0% ± 2.6% of control, n = 5, p < 0.001; Figures 4C and 4D). Because bath application affected both presynaptic and postsynaptic channels, it may enhance transmitter release from DA neuron terminals; indeed, depolarization due to glutamate cotransmission was enhanced with apamin application (172.0% ± 15.4% of control, n = 5, p = 0.010). The smaller effect of apamin compared to intracellular BAPTA could be due to enhanced DA release. The simultaneous application of a cocktail of D2, mACh, and SK channel antagonists eliminated the PBH almost completely (4.8% ± 0.9% of control, n = 5, p < 0.001; Figures 4C and 4D). Thus, activation of DA neuron inputs to the m-shell evokes in ChIs a glutamate-mediated burst followed by a hyperpolarization mediated by SK channels, augmented by D2 and muscarinic actions.

Heterogeneity in DA Neuron-ChI Synaptic Connections Is due to Glutamate Cotransmission

Because ChIs in all striatal domains exhibited a DA D2-mediated inhibitory response to train photostimulation of DA neuron inputs, the heterogeneity in the DA neuron signal across domains is likely due to glutamate cotransmission. Indeed, medial VTA DA neurons that innervate the m-shell preferentially express the vesicular glutamate transporter 2 (VGLUT2) (Li et al., 2013), which mediates glutamate cotransmission. To test this, we used mice with a conditional knockout (cKO) of VGLUT2 in DA neurons to eliminate glutamate cotransmission (Hnasko et al., 2010). Although slices from littermate controls showed regional heterogeneity in ChI responses, in VGLUT2 cKO slices, train photostimulation produced a reduction or pause in ChI firing across all three Str domains (Figures 5A and 5B). In the dStr, the same pause was seen in control and VGLUT2 cKO (firing ratio: control 0.13 ± 0.04, n = 5 cells; cKO 0.08 ± 0.06, n = 5 cells; p = 0.31, Mann-Whitney U test; Figure 5B), confirming the lack of significant glutamate cotransmission. In the core, the subtle inhibition in control became a pause in VGLUT2 cKO (firing ratio: control 0.97 ± 0.15, n = 4 cells; cKO 0.14 ± 0.10, n = 5 cells; p = 0.016; Figure 5B), showing that modest glutamate cotransmission in the core is obscured by DA/GABA-mediated inhibition. In the m-shell, the burst followed by inhibition in control slices became pure inhibition in VGLUT2 cKO (firing ratio control 4.1 ± 0.6, n = 5 cells; cKO 0.55 ± 0.11, n = 5 cells; p = 0.009; Figure 5B). The PBH was not significantly reduced (control −6.0 ± 1.9 mV, n = 5 cells; cKO 2.9 ± 0.9 mV, n = 5 cells; p = 0.17; Figure 5C), probably due to the D2-mediated component. Under

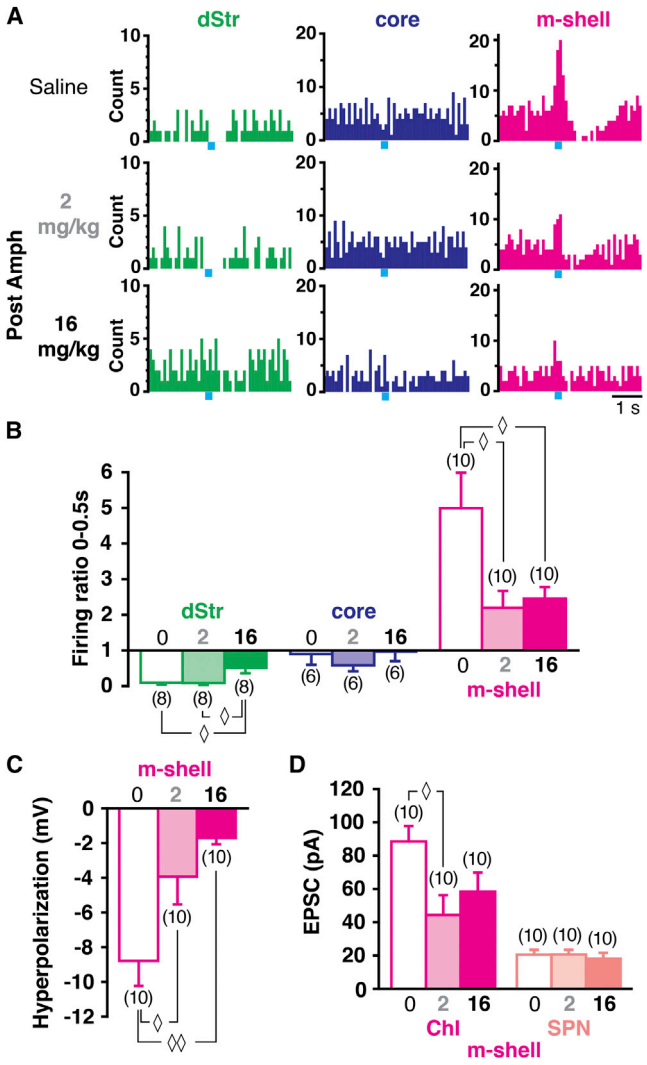

Figure 6. Amphetamine-Induced Plasticity Is Regionally Heterogeneous

(A) Peristimulus histograms of firing in the three regions in mice previously treated with saline (top), low-dose (middle), and high-dose (bottom) amphetamine.

(B) Firing ratio measurements following saline (open bars), low-dose (light-shaded bars) or high-dose (dark-shaded bars) show that low-dose attenuates ChI bursts selectively in the m-shell, while high-dose attenuates ChI bursts in the dStr.

(C) The PBH in the m-shell shows a progressive dose-dependent reduction.

(D) EPSCs evoked by single-pulse photostimulation (at 0.1 Hz) in m-shell ChIs were attenuated following amphetamine, whereas there was no effect in SPNs. ◇ and ◇ ◇ indicate $p < 0.05$ and $p < 0.01$, respectively, by one-way ANOVA with Scheffe's post hoc test.

Data are presented as mean ± SEM. See also Figure S4.

voltage clamp, fast EPSCs observed in control (111.5 ± 35.7 pA, n = 5 cells) were completely eliminated in VGLUT2 cKO (1.3 ± 0.4 pA, n = 5 cells; p = 0.009; Figure 5D), confirming that the fast EPSCs were mediated by glutamate cotransmission. Although DA-mediated inhibition in ChIs was observed in all three striatal domains, the glutamate-mediated excitation showed a strong regional gradient, strongest in the m-shell, weak in the core and absent in the dStr. Thus, regional heterogeneity in DA neuron actions was due mainly to glutamate cotransmission.

DA Neuron-ChI Synaptic Connections Show Regionally Heterogeneous Plasticity

If DA neuron-ChI synaptic connections are important for striatal function, we should expect to see that the connections are plastic, and moreover that they demonstrate regional heterogeneity of functionally relevant plasticity. A single psychostimulant dose causes distributed synaptic changes in the mesolimbic DA system (Belin et al., 2009; Lüscher and Malenka, 2011). So we examined the DA neuron-ChI synaptic connection following a single low or high dose of amphetamine. It is well established that low-dose amphetamine induces hyperlocomotion via DA release in the NAc, whereas with high dose, locomotion gives way to stereotypy via DA release in the dStr (Kelly et al., 1975; Yates et al., 2007). To modify circuitry in the NAc and the dStr differentially (Yates et al., 2007), we used 2 mg/kg as low dose and 16 mg/kg as high dose, respectively. We confirmed the dose dependence by observation of hyperlocomotion or grooming stereotypy (Figures S4B and S4C).

After amphetamine-induced behaviors had subsided, we measured DA neuron input to ChIs in brain slices (Figure S4A). In low-dose slices, the burst in m-shell ChIs was reduced (firing ratio saline 5.0 ± 1.0, low dose 2.2 ± 0.5, p = 0.022, one-way ANOVA with Scheffe's post hoc test), whereas there was no significant effect in the core (saline 0.90 ± 0.30, low dose 0.58 ± 0.17, p = 0.71) or the dStr (saline 0.095 ± 0.052, low dose 0.086 ± 0.056, p = 0.99; Figures 6A and 6B). In high-dose slices, both the burst in the m-shell (2.5 ± 0.3) and the pause in the dStr (0.51 ± 0.15) were reduced (m-shell p = 0.040, dStr p = 0.021), whereas there was no significant effect in the core (1.0 ± 0.3, p = 0.97; Figures 6A and 6B). The burst in the m-shell was not reduced further, comparing low to high dose (p = 0.96), whereas the pause in the dStr was significantly reduced in high dose (p = 0.019; Figures 6A and 6B). Baseline firing frequencies were not affected (Figure S4D), suggesting that the effects were principally synaptic. The amplitude of the PBH in the m-shell was reduced by low dose (saline 8.8 ± 1.4 mV, low dose 3.9 ± 1.6 mV, p = 0.038), and further reduced by high dose (high dose 1.7 ± 0.4 mV, p = 0.002 compared to saline, p = 0.038 compared to low dose; Figure 6C). DA neuron EPSCs in m-shell ChIs were significantly reduced by low dose (saline 88.5 ± 9.3 pA, low dose 44.4 ± 11.9 pA, p = 0.025), but not reduced further by high dose (58.3 ± 11.5 pA, p = 0.67, compared to low dose; Figure 6D). As both fast EPSCs and bursts in ChIs were eliminated by VGLUT2 cKO (Figure 5), the reduction in bursts with low dose was due to attenuation of glutamate cotransmission.

Because there was no further reduction in EPSC amplitude with high dose, the attenuation of the PBH was not due to further reduction of glutamate cotransmission, implying that the further reduction with high dose involves a reduction in the D2 component of the PBH (Figure 4D). No amphetamine effect was observed in m-shell SPNs, with either low or high dose (p = 0.64; Figure 6D), indicating that amphetamine preferentially

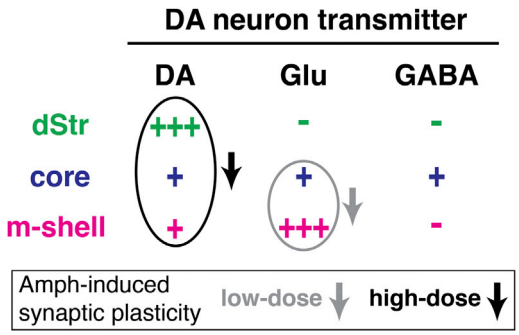

Figure 7. Regional Heterogeneity of Fast DA Neuron Transmission to ChIs Is Accentuated by Amphetamine

Fast synaptic actions of DA neurons on ChIs are mediated by DA, glutamate, and GABA. The strength of connections is indicated by the number of plus signs. Ovals and arrows indicate differential attenuation of synaptic effects following low-dose or high-dose amphetamine.

affects DA neuron connections to ChIs. Effects in the core were difficult to discern, given the small responses of ChIs under control conditions. Thus low-dose amphetamine attenuated glutamate cotransmission mainly in the m-shell, whereas high dose attenuated both DA and glutamate transmission, and this extended to attenuation of DA transmission in the dStr.

DISCUSSION

DA has been thought to have principally modulatory actions in striatal projection areas. However, DA neurons fire in patterns that also transmit more discrete temporal information. Such information could be conveyed by glutamate (Stuber et al., 2010; Tecuapetla et al., 2010) or GABA (Tritsch et al., 2012) cotransmission to SPNs. We have now shown that DA neurons convey discrete temporal information to ChIs via fast DAergic IPSPs in ChIs in the dStr and robust glutamatergic EPSPs in ChIs in the m-shell. In the core, they have a more subtle action. Behaviorally relevant bursts in DA neurons produce a timed pause in ChI firing in the dStr mediated by DA action at D2 receptors, robust excitation in ChIs in the m-shell mediated by glutamate acting at both AMPA and NMDA receptors, followed by a pause mainly driven by activity-dependent currents and DA, and more modest inhibition in the core mediated by D2 and $GABA_A$ inhibition countered by modest glutamatergic action (Figure 7). This striking regional heterogeneity counters the view that DA neurons have homogeneous actions across striatal domains. A single dose of amphetamine accentuates this heterogeneity through a region- and dose-dependent reduction in the DA-neuron control of ChI firing (Figure 7, arrows) indicating that the connections are likely to mediate an early step in drug-induced plasticity.

Fast DA Neuron Signaling to dStr ChIs

Fast DA neuron IPSCs are seen in SN DA neurons (Beckstead et al., 2004; Gantz et al., 2013) but have not been reported previously in DA neuron projection areas. In contrast to the modulatory actions of DA on SPNs, the present results reveal that DA neurons projecting to ChIs mediate a fast D2-mediated IPSC, most prominent in the dStr and weaker and slower in the NAc. The short latency of the DAergic IPSC in dStr ChIs (about 5 ms) is remarkable for a G protein-coupled receptor (GPCR)-mediated response, and significantly faster than the DA IPSC in SN DA neurons (about 50 ms) (Beckstead et al., 2004; Gantz et al., 2013). However, the speed of activation of GPCR-mediated responses depends on concentration and diffusion of transmitters (Lohse et al., 2007); once the transmitter has bound, signal transduction may take as little as 1 ms, as exemplified by rhodopsin activation, for a direct-coupled response (Lohse et al., 2007). This would argue that the D2-mediated IPSP in dStr ChIs is likely mediated via $\beta\gamma$ subunit direct activation of GIRKs (Whorton and MacKinnon, 2013). The DA neuron elicited IPSC in ChIs is not that much faster than the Ca^{2+} rise in a proximate cortical dendritic spine elicited by DA uncaging, which requires about 30 ms (Araya et al., 2013), when the additional time required for G protein subunit diffusion and Ca^{2+} release is factored in. Thus, the short-latency D2 activation of GIRKs in ChIs we have seen appears plausible for an axodendritic (Dimova et al., 1993) synaptic response. Although DA produces a discrete IPSP in ChIs, the response is slower than that mediated by ionotropic receptors; as a result, DA neuron bursts are converted into an integrated hyperpolarization with relatively fast onset in dStr ChIs.

DA neurons generate large $GABA_A$ IPSCs in dStr SPNs (Tritsch et al., 2012), but these are not seen in ChIs. There may be a modest DA neuron $GABA_A$ input to ChIs in the dStr, which was not large enough to reduce firing. A small IPSC did remain 5 min after intracellular dialysis with Cs^+ that could be $GABA_A$ mediated; however, it is more likely that the Cs^+ did not reach more distal dendrites and so did not fully block the GIRK-mediated response. It is striking that in the dStr DA neuron GABAergic synaptic actions are seen in SPNs but not in ChIs. This suggests that presynaptic plasma membrane GABA transporters or postsynaptic $GABA_A$ receptors are distributed to DA neuron synaptic connections with SPNs and away from synaptic connections with ChIs.

When DA neurons fire in bursts, ChIs pause (Schulz and Reynolds, 2013). Several mechanisms have been proposed for the generation of the ChI pauses, but direct DA neuron actions have not been considered. For example, cortical inputs could trigger hyperpolarization-activated cation channels or enhance slow afterhyperpolarizations (Oswald et al., 2009; Wilson and Goldberg, 2006), or thalamic inputs could augment DA release (Ding et al., 2010), but these require preceding glutamatergic input. Our observations show that DA neuron DA transmission is sufficient to pause ChIs in the dStr and could thus drive the inverse correlation between DA neuron firing and ChI pauses directly. ChIs trigger DA release via presynaptic action on DA neuron terminals (Threlfell et al., 2012), so a DA neuron-driven pause in ChIs would reduce ChI-driven DA release and help to terminate the pause. In this way, DA neuron activity could accentuate the oscillation of ChIs between firing and pauses.

DA Neuron Responses in ChIs in the NAc

In the m-shell, DA neuron bursts reliably drove a burst-pause sequence in ChIs. In all ChIs recorded in the m-shell under control conditions, train photostimulation of DA neuron terminals elicited a burst, showing the reliable translation of DA-neuron

bursts into ChI bursts. As is characteristic of ionotropic glutamate transmission, both the onset and offset of the response was fast so the timing of DA-neuron bursting was precisely transmitted to ChIs. By comparison, glutamate cotransmission in SPNs was weak. So together with the more hyperpolarized resting membrane potential of SPNs (Kreitzer, 2009), DA neuron glutamate cotransmission should only trigger SPN spikes in concert with other excitatory inputs (Chuhma et al., 2004; Tecuapetla et al., 2010). In contrast, DA neuron input alone is sufficient to drive ChIs to fire, indicating that ChIs are more likely targets of discrete temporal information encoded in DA neuron firing. When DA neurons fire synchronously to salient stimuli (Schultz, 2013), their excitatory actions are likely to entrain ChI burst-pause sequences specifically in the m-shell.

The robust PBH in m-shell ChIs was driven by a combination of direct synaptic and activity-dependent mechanisms, involving D2 and mACh receptors, and SK channels. These mechanisms likely interact synergistically. In rat striatal ChIs, D2 receptor activation inhibits N-type voltage gated Ca^{2+} channels (Momiyama and Koga, 2001), which may in turn reduce SK channel activation. mACh receptors may directly modulate SK channels through mACh, as is seen in hippocampal neurons (Giessel and Sabatini, 2010). Considering the widespread influence of ChIs (Goldberg and Wilson, 2010; Kreitzer, 2009), timing-dependent DA neurons actions may more effectively control striatal circuitry by controlling ChI activity.

In the core, the DA neuron action on ChIs was weak and variable. Single-pulse photostimulation did not elicit a reliable response, but train photostimulation slowed ChI firing, via D2 and $GABA_A$ mediation. The $GABA_A$ hyperpolarization was not always apparent, but it significantly slowed firing. Most likely it was mediated by DA neuron GABA cotransmission (Tritsch et al., 2012), but it could also be mediated polysynaptically by striatal GABA neurons (SPNs or interneurons). A modest glutamatergic contribution was revealed by the change in the ChI response from a small reduction in firing to a pause in cKO slices. Firing attenuation in core ChIs thus involves a slight imbalance in inhibition (DA and GABA) and excitation (glutamate), favoring inhibition.

Amphetamine-Induced Heterogeneous Plasticity of DA Neuron-ChI Transmission

Amphetamine dose-dependently attenuated DA neuron inputs to ChIs with regional heterogeneity, consistent with the involvement of different Str subregions in amphetamine-dependent behaviors (Kelly et al., 1975). After acute behavioral effects of low-dose amphetamine had subsided, we found that the DA neuron elicited ChI bursts were diminished in the m-shell. As a result, DA neurons selectively lost the ability to synchronize bursts in m-shell ChIs. The ensuing ChI pause was also reduced, presumably due to a diminution in the activity-dependent component of the PBH. In contrast, high-dose amphetamine attenuated pauses in both m-shell and dStr, presumably due to a diminution in DA signaling. Regionally, amphetamine would be expected to have its strongest action in the dStr where DA transporter (DAT) expression is highest (Ciliax et al., 1995). However, the dose-dependent behavioral effects of amphetamine follow a ventral-to-dorsal progression (Belin et al., 2009; Di Chiara and Imperato, 1988; Kelly et al., 1975). Possibly, DA neuron glutamate cotransmission to ChIs in the NAc medial-shell contributes to the observed regional differences in the behavioral actions of acute amphetamine.

VGLUT2 cKO mice respond less to acute administration of cocaine (Hnasko et al., 2010) and amphetamine (Birgner et al., 2010). The DAT-driven conditional deletion of VGLUT2 is restricted to DA neurons and further restricted to medial VTA DA neurons by the predominant medial distribution of the VGLUT2-expressing DA neurons (Li et al., 2013). Glutamatergic cotransmission is strongest in the NAc m-shell, and in the m-shell strongest onto ChIs, arguing that the behavioral phenotype of VGLUT2 cKO mice is due to the loss of DA neuron glutamatergic cotransmission to m-shell ChIs. The modest reduction in DA neuron number seen in VGLUT2 cKO mice (Bérubé-Carrière et al., 2012) could contribute to the attenuated stimulant response, but this is countered by the selective impact of amphetamine on DA neuron connections to m-shell ChIs, and not SPNs (Ishikawa et al., 2013). The selective susceptibility of DA neuron glutamatergic connections to ChIs identifies the connections as a primary target of psychostimulant action and argues that they play a crucial role in the initiation of drug-induced changes in the striatal circuitry.

Implications for Striatal Circuit Function

Pauses in ChI firing appear to parse behavioral sequences and show progressive synchronization with learning (Graybiel et al., 1994). DA neuron bursts could mediate such a plastic process uniquely in the m-shell and underlie reward-related learning. Indeed, nicotine—another addictive drug—synchronizes VTA DA neuron firing (Li et al., 2011), which could then entrain ChIs in the m-shell to drive pathological learning and addictive behavior. In contrast, the fast DA response in the dStr, which is not as fast as glutamate cotransmission, may work in concert with other inputs to synchronize ChI firing. Consistent with this, the burst-pause sequence in m-shell ChIs closely resembles the combination of thalamic input and DA input seen in the dStr in response to salient information (Ding et al., 2010).

The intrinsic properties of DA neurons vary across the ventral midbrain (Fields et al., 2007; Roeper, 2013). We now show that this heterogeneity extends dramatically to their synaptic connections in the Str. Although DA appears to exert modulatory actions on all Str neurons, DA neurons signal with fast temporally discrete signals to ChIs and so have a unique conduit to the control of Str function through their connections to ChIs. ChIs are dominant Str interneurons with widespread influence, so control of ChIs allows DA neurons to exert timing-dependent control of the striatal circuitry. DA neurons may thus use ChIs as effective entry points—with prominent, regionally heterogeneous and plastic fast inputs—to orchestrate striatal circuit function.

EXPERIMENTAL PROCEDURES

Experimental Animals

Mice were handled in accordance with the guidelines of the National Institutes of Health *Guide for the Care and Use of Laboratory Animals*, under protocols approved by the Institutional Animal Care and Use Committees of Columbia University and New York State Psychiatric Institute. C57/BL6J background hemizygous DAT-internal ribosome entry site (IRES) cre mice (Bäckman

et al., 2006) (Jackson Laboratory, stock number 006660) were used. VGLUT2 cKO mice were obtained by breeding floxed VGLUT2 mice (Hnasko et al., 2010) with DAT-IRES-cre mice. See also Supplemental Experimental Procedures.

AAV-cre-Inducible-ChR2-EYFP Injection

To express ChR2 in DA neurons selectively, we injected adeno-associated virus (AAV) serotype 5 encoding *ChR2* fused to *EYFP* (*AAV5-EF1a-DIO-ChR2(H134R)-EYFP*) into DAT-IRES-cre mice. Mice (ages postnatal days 28–40 [P28–P40], n = 95) were anesthetized with Ketamine (90 mg/kg) + Xylazine (7 mg/kg). A glass pipette (PCR micropipettes, Drummond), pulled to a tip diameter ~20 μm, was lowered to just above the ventral midbrain (coordinates relative to bregma: −3.3 mm anteroposterior, −4.3 mm dorsoventral, and 0.5 mm lateral) and pressure injections of 1 μl of AAV5-EF1a-DIO-ChR2-EYFP (titer 1.5 × 10^{12} virus molecules/ml) were made. The pipette was left in place for ~3 min to minimize backflow along the injection tract, then withdrawn, and the mouse was allowed to recover.

Immunohistochemistry

Mice 50–55 days postviral injection (P90) were anesthetized with ketamine (100 mg/kg) + xylazine (15 mg/kg), and rapidly perfused intracardially with 1 ml of warm phosphate buffer solution (PBS; 0.1 M [pH 7.4]) containing heparin (10,000 IU/L), then with 5 ml cold PBS, followed by 5 ml 4% paraformaldehyde in PBS. After overnight postfixation at 4°C, brains were sliced with a vibrating microtome (Leica VT1200), and 50 μm coronal slices were collected into a cryoprotectant solution (30% glycerol, 30% ethylene glycol in 0.1 M Tris HCl [pH 7.4]) and kept at −20°C until processing. Glycine (100 mM) for 30 min was used to quench the aldehydes. Nonspecific binding was blocked with 10% normal goat serum (Millipore) in 0.1% Triton X-100 for 2 hr. Brain slices were incubated with a pair of primary antibodies either anti-TH (mouse monoclonal, 1:10,000, MAB318, Millipore) and anti-GFP (rabbit polyclonal, 1:2,000, AB3080, Millipore), or anti-GFP (1:2,000) and anti-GAD 67 (mouse monoclonal, 1:1,000, MAB5406, Millipore) in 0.02% Triton X-100 and 2% normal goat serum solution on a shaker at 4°C for 48 hr. Sections were then washed with PBS and incubated for 45 min with one of the following pairs of secondary antibodies: anti-mouse Alexa Fluor 594 or Alexa Fluor 555 and anti-rabbit Alexa Fluor 488 (made in goat, 1:200, Invitrogen) in 0.02% Triton X-100. Brain sections were mounted using Prolong Gold (Invitrogen) and stored at 4°C. Photomicrographs were acquired using a FluoView FV1000 confocal laser-scanning microscope (Olympus) or Nikon A1 confocal laser-scanning microscope (Nikon Instruments), a 60× oil objective (n.a. 1.42) and the 488 and 559 nm channels.

Slice Electrophysiology

Recordings were done 21–44 days after viral injection (ages P55–P72). Coronal slices through the striatum, 300 μm thick, were prepared as described previously (Chuhma et al., 2011). After 1 hr incubation at room temperature to allow slices to recover, slices were placed in a recording chamber with continuous perfusion of artificial cerebrospinal fluid (without any drugs), saturated with carbogen (95% O_2 + 5% CO_2), and maintained at ~32°C (TC 344B Temperature Controller, Warner Instruments). Expression of ChR2 was confirmed by visualization of YFP fluorescence in DA neuron axons and varicosities. Recordings were done in regions with bright YFP fluorescence. Whole-cell patch recording followed standard techniques using glass pipettes (3–6 MΩ). The intracellular solution contained (in mM): 140 K^+-gluconate, 10 HEPES, 0.1 $CaCl_2$, 2 $MgCl_2$, 1 EGTA, 2 ATP-Na_2 and 0.1 GTP-Na_2 (pH 7.3). Recording was done with Axopatch 200B amplifier (Molecular Devices) under voltage clamp (holding potential = −70 mV, unless otherwise noted) or fast current clamp mode. For voltage clamp recording, series resistance (9–35 MΩ) was compensated online by 70%–80%. Liquid junction potential (~12 mV) was adjusted online. ChR2 responses were evoked by field illumination with a high-power blue (470 nm) LED (Thorlabs) delivered either as a single 5 ms pulse at 0.1 Hz or in a train of five pulses at 20 Hz at 30 s intervals. For pharmacological studies, SR95531 (Tocris Bioscience), CGP 55345 (Tocris), 6-cyano-7-nitroquinoxaline-2,3-dione (CNQX, Sigma-Aldrich), D-(-)-2-Amino-5-phosphonopentanoic acid (D-APV, Tocris), SCH23390 (Sigma-Aldrich), Sulpiride (Tocris), Scopolamine (Tocris), or apamin (Sigma-Aldrich) were delivered by perfusion. For inactivation of G proteins in recorded neurons, the GTP in pipette solution was replaced with GDPβS (trilithium salt) 1–1.5 mM (Sigma-Aldrich); QX-314 (lidocaine N-ethyl bromide) 5 mM (Tocris) was added to block spontaneous firing for accurate measurement of IPSP amplitude. GDPβS solutions were made from powder just before recording. For intracellular effect of Cs^+, K^+-gluconate was replaced with Cs^+-gluconate and QX-314 was added (pH was adjusted with CsOH). Control experiments for GDPβS and intracellular Cs^+ effects were done with K^+-gluconate pipette solution with QX-314 in separate sets of neurons. For intracellular free Ca^{2+} chelation, EGTA in the intracellular solution was replaced with BAPTA (1,2-Bis(2-aminophenoty)ethane-N,N,N',N'-tetraacetic acid; Tocris) 10 mM, K^+-gluconate was reduced to 130 mM to adjust osmolality and pH adjusted with KOH. Intracellular BAPTA started to show its effect 5 min after entering whole-cell mode, so the first 5 min served as control; after 10 min, full effects were achieved. The PBH in m-shell was measured as the negative peak 0.5–1.5 s after the onset of photostimulation.

Data Analysis and Statistics

Electrophysiological data were filtered at 5 kHz with a 4-pole Bessel filter and digitized at 200 μs sample intervals (ITC-16 Interface, ALA Scientific Instruments). Acquisition and analysis were done with AxoGraph X (AxoGraph Scientific). Peak amplitudes of synaptic responses were measured from averages of ten individual traces. Latency of PSPs was measured as the time from the onset of photostimulation to 5% of the peak response. PSC rise time was measured as the time from 10%–90% of peak amplitude. Baseline firing frequencies were calculated as average frequency in a 2 s window of baseline obtained from ten consecutive traces. Effects of train photostimulation on ChIs were evaluated as the firing ratio of firing frequency during the 0.5 s window from the onset of the photostimulation to the preceding baseline. Statistical analyses were done in SPSS 20 (IBM). For comparison of three values, one-way ANOVA was used, and significance of differences evaluated using Scheffe's post hoc test. For comparison of two values or comparisons to baseline levels, Student's t test or one-sample t test were used for data with $n \geq 10$; nonparametric tests were used for data with $n < 10$.

SUPPLEMENTAL INFORMATION

Supplemental Information includes Supplemental Experimental Procedures and four figures and can be found with this article online at http://dx.doi.org/10.1016/j.neuron.2013.12.027.

ACKNOWLEDGMENTS

We thank Karl Deisseroth for the DIO-ChR2-EYFP plasmid; the Vector Core Facility, University of North Carolina for packaging the viral vector; Tom Hnasko, Robert Edwards, and Richard Palmiter for flox-VGLUT2 mice; and Mark Ansorge, René Hen, Jonathan Javitch, Christoph Kellendonk, and David Sulzer for discussions. We thank Celia Gellman, Yvonne Wang, Andra Mihali, and Bianca Field for technical assistance. This work was supported by NIMH P50 MH086404 (to S.R. and H.M.), NIDA R01 DA017978 (to S.R.), and a NARSAD Young Investigator Award from the Brain & Behavior Research Foundation (to S.M.).

Accepted: December 19, 2013
Published: February 19, 2014

REFERENCES

Araya, R., Andino-Pavlovsky, V., Yuste, R., and Etchenique, R. (2013). Two-photon optical interrogation of individual dendritic spines with caged dopamine. ACS Chem. Neurosci. *4*, 1163–1167.

Atasoy, D., Aponte, Y., Su, H.H., and Sternson, S.M. (2008). A FLEX switch targets Channelrhodopsin-2 to multiple cell types for imaging and long-range circuit mapping. J. Neurosci. *28*, 7025–7030.

Bäckman, C.M., Malik, N., Zhang, Y., Shan, L., Grinberg, A., Hoffer, B.J., Westphal, H., and Tomac, A.C. (2006). Characterization of a mouse strain

expressing Cre recombinase from the 3′ untranslated region of the dopamine transporter locus. Genesis *44*, 383–390.

Beckstead, M.J., Grandy, D.K., Wickman, K., and Williams, J.T. (2004). Vesicular dopamine release elicits an inhibitory postsynaptic current in midbrain dopamine neurons. Neuron *42*, 939–946.

Belin, D., Jonkman, S., Dickinson, A., Robbins, T.W., and Everitt, B.J. (2009). Parallel and interactive learning processes within the basal ganglia: relevance for the understanding of addiction. Behav. Brain Res. *199*, 89–102.

Benarroch, E.E. (2012). Effects of acetylcholine in the striatum. Recent insights and therapeutic implications. Neurology *79*, 274–281.

Bérubé-Carrière, N., Guay, G., Fortin, G.M., Kullander, K., Olson, L., Wallén-Mackenzie, A., Trudeau, L.E., and Descarries, L. (2012). Ultrastructural characterization of the mesostriatal dopamine innervation in mice, including two mouse lines of conditional VGLUT2 knockout in dopamine neurons. Eur. J. Neurosci. *35*, 527–538.

Birgner, C., Nordenankar, K., Lundblad, M., Mendez, J.A., Smith, C., le Grevès, M., Galter, D., Olson, L., Fredriksson, A., Trudeau, L.E., et al. (2010). VGLUT2 in dopamine neurons is required for psychostimulant-induced behavioral activation. Proc. Natl. Acad. Sci. USA *107*, 389–394.

Brown, M.T.C., Tan, K.R., O'Connor, E.C., Nikonenko, I., Muller, D., and Lüscher, C. (2012). Ventral tegmental area GABA projections pause accumbal cholinergic interneurons to enhance associative learning. Nature *492*, 452–456.

Cachope, R., Mateo, Y., Mathur, B.N., Irving, J., Wang, H.-L., Morales, M., Lovinger, D.M., and Cheer, J.F. (2012). Selective activation of cholinergic interneurons enhances accumbal phasic dopamine release: setting the tone for reward processing. Cell Rep. *2*, 33–41.

Chuhma, N., Tanaka, K.F., Hen, R., and Rayport, S. (2011). Functional connectome of the striatal medium spiny neuron. J. Neurosci. *31*, 1183–1192.

Chuhma, N., Zhang, H., Masson, J., Zhuang, X., Sulzer, D., Hen, R., and Rayport, S. (2004). Dopamine neurons mediate a fast excitatory signal via their glutamatergic synapses. J. Neurosci. *24*, 972–981.

Ciliax, B.J., Heilman, C., Demchyshyn, L.L., Pristupa, Z.B., Ince, E., Hersch, S.M., Niznik, H.B., and Levey, A.I. (1995). The dopamine transporter: immunochemical characterization and localization in brain. J. Neurosci. *15*, 1714–1723.

Di Chiara, G. (2002). Nucleus accumbens shell and core dopamine: differential role in behavior and addiction. Behav. Brain Res. *137*, 75–114.

Di Chiara, G., and Imperato, A. (1988). Drugs abused by humans preferentially increase synaptic dopamine concentrations in the mesolimbic system of freely moving rats. Proc. Natl. Acad. Sci. USA *85*, 5274–5278.

Dimova, R., Vuillet, J., Nieoullon, A., and Kerkerian-Le Goff, L. (1993). Ultrastructural features of the choline acetyltransferase-containing neurons and relationships with nigral dopaminergic and cortical afferent pathways in the rat striatum. Neuroscience *53*, 1059–1071.

Ding, J.B., Guzman, J.N., Peterson, J.D., Goldberg, J.A., and Surmeier, D.J. (2010). Thalamic gating of corticostriatal signaling by cholinergic interneurons. Neuron *67*, 294–307.

Do, J., Kim, J.I., Bakes, J., Lee, K., and Kaang, B.K. (2012). Functional roles of neurotransmitters and neuromodulators in the dorsal striatum. Learn. Mem. *20*, 21–28.

Fields, H.L., Hjelmstad, G.O., Margolis, E.B., and Nicola, S.M. (2007). Ventral tegmental area neurons in learned appetitive behavior and positive reinforcement. Annu. Rev. Neurosci. *30*, 289–316.

Gantz, S.C., Bunzow, J.R., and Williams, J.T. (2013). Spontaneous inhibitory synaptic currents mediated by a G protein-coupled receptor. Neuron *78*, 807–812.

Giessel, A.J., and Sabatini, B.L. (2010). M1 muscarinic receptors boost synaptic potentials and calcium influx in dendritic spines by inhibiting postsynaptic SK channels. Neuron *68*, 936–947.

Goldberg, J.A., and Wilson, C.J. (2010). The cholinergic interneurons of the striatum: intrinsic properties underlie multiple discharge patterns. In Handbook of Behavioral Neuroscience, S. Heinz and Y.T. Kuei, eds. (New York: Elsevier), pp. 133–149.

Graybiel, A.M., Aosaki, T., Flaherty, A.W., and Kimura, M. (1994). The basal ganglia and adaptive motor control. Science *265*, 1826–1831.

Hnasko, T.S., Chuhma, N., Zhang, H., Goh, G.Y., Sulzer, D., Palmiter, R.D., Rayport, S., and Edwards, R.H. (2010). Vesicular glutamate transport promotes dopamine storage and glutamate corelease in vivo. Neuron *65*, 643–656.

Ikemoto, S. (2007). Dopamine reward circuitry: two projection systems from the ventral midbrain to the nucleus accumbens-olfactory tubercle complex. Brain Res. Brain Res. Rev. *56*, 27–78.

Ishikawa, M., Otaka, M., Neumann, P.A., Wang, Z., Cook, J.M., Schlüter, O.M., Dong, Y., and Huang, Y.H. (2013). Exposure to cocaine regulates inhibitory synaptic transmission from the ventral tegmental area to the nucleus accumbens. J. Physiol. *591*, 4827–4841.

Kelly, P.H., Seviour, P.W., and Iversen, S.D. (1975). Amphetamine and apomorphine responses in the rat following 6-OHDA lesions of the nucleus accumbens septi and corpus striatum. Brain Res. *94*, 507–522.

Kreitzer, A.C. (2009). Physiology and pharmacology of striatal neurons. Annu. Rev. Neurosci. *32*, 127–147.

Li, W., Doyon, W.M., and Dani, J.A. (2011). Acute in vivo nicotine administration enhances synchrony among dopamine neurons. Biochem. Pharmacol. *82*, 977–983.

Li, X., Qi, J., Yamaguchi, T., Wang, H.-L., and Morales, M. (2013). Heterogeneous composition of dopamine neurons of the rat A10 region: molecular evidence for diverse signaling properties. Brain Struct. Funct. *218*, 1159–1176.

Lohse, M.J., Hoffmann, C., Nikolaev, V.O., Vilardaga, J.P., and Bünemann, M. (2007). Kinetic analysis of G protein-coupled receptor signaling using fluorescence resonance energy transfer in living cells. Adv. Protein Chem. *74*, 167–188.

Lüscher, C., and Malenka, R.C. (2011). Drug-evoked synaptic plasticity in addiction: from molecular changes to circuit remodeling. Neuron *69*, 650–663.

Momiyama, T., and Koga, E. (2001). Dopamine D_2-like receptors selectively block N-type Ca_{2+} channels to reduce GABA release onto rat striatal cholinergic interneurones. J. Physiol. *533*, 479–492.

Oswald, M.J., Oorschot, D.E., Schulz, J.M., Lipski, J., and Reynolds, J.N.J. (2009). I_H current generates the afterhyperpolarisation following activation of subthreshold cortical synaptic inputs to striatal cholinergic interneurons. J. Physiol. *587*, 5879–5897.

Prakash, R., Yizhar, O., Grewe, B., Ramakrishnan, C., Wang, N., Goshen, I., Packer, A.M., Peterka, D.S., Yuste, R., Schnitzer, M.J., and Deisseroth, K. (2012). Two-photon optogenetic toolbox for fast inhibition, excitation and bistable modulation. Nat. Methods *9*, 1171–1179.

Rivera, A., Alberti, I., Martín, A.B., Narváez, J.A., de la Calle, A., and Moratalla, R. (2002). Molecular phenotype of rat striatal neurons expressing the dopamine D5 receptor subtype. Eur. J. Neurosci. *16*, 2049–2058.

Roeper, J. (2013). Dissecting the diversity of midbrain dopamine neurons. Trends Neurosci. *36*, 336–342.

Schultz, W. (2013). Updating dopamine reward signals. Curr. Opin. Neurobiol. *23*, 229–238.

Schulz, J.M., and Reynolds, J.N. (2013). Pause and rebound: sensory control of cholinergic signaling in the striatum. Trends Neurosci. *36*, 41–50.

Stuber, G.D., Hnasko, T.S., Britt, J.P., Edwards, R.H., and Bonci, A. (2010). Dopaminergic terminals in the nucleus accumbens but not the dorsal striatum corelease glutamate. J. Neurosci. *30*, 8229–8233.

Tecuapetla, F., Patel, J.C., Xenias, H., English, D., Tadros, I., Shah, F., Berlin, J., Deisseroth, K., Rice, M.E., Tepper, J.M., and Koos, T. (2010). Glutamatergic signaling by mesolimbic dopamine neurons in the nucleus accumbens. J. Neurosci. *30*, 7105–7110.

Threlfell, S., Lalic, T., Platt, N.J., Jennings, K.A., Deisseroth, K., and Cragg, S.J. (2012). Striatal dopamine release is triggered by synchronized activity in cholinergic interneurons. Neuron *75*, 58–64.

Tritsch, N.X., Ding, J.B., and Sabatini, B.L. (2012). Dopaminergic neurons inhibit striatal output through non-canonical release of GABA. Nature *490*, 262–266.

Tsai, H.C., Zhang, F., Adamantidis, A., Stuber, G.D., Bonci, A., de Lecea, L., and Deisseroth, K. (2009). Phasic firing in dopaminergic neurons is sufficient for behavioral conditioning. Science *324*, 1080–1084.

Whorton, M.R., and MacKinnon, R. (2013). X-ray structure of the mammalian GIRK2-$\beta\gamma$ G-protein complex. Nature *498*, 190–197.

Wilson, C.J., and Goldberg, J.A. (2006). Origin of the slow afterhyperpolarization and slow rhythmic bursting in striatal cholinergic interneurons. J. Neurophysiol. *95*, 196–204.

Yan, Z., and Surmeier, D.J. (1997). D5 dopamine receptors enhance Zn^{2+}-sensitive $GABA_A$ currents in striatal cholinergic interneurons through a PKA/PP1 cascade. Neuron *19*, 1115–1126.

Yates, J.W., Meij, J.T.A., Sullivan, J.R., Richtand, N.M., and Yu, L. (2007). Bimodal effect of amphetamine on motor behaviors in C57BL/6 mice. Neurosci. Lett. *427*, 66–70.

Yizhar, O., Fenno, L.E., Davidson, T.J., Mogri, M., and Deisseroth, K. (2011). Optogenetics in neural systems. Neuron *71*, 9–34.